PROCEEDINGS OF SPIE

SPIEDigitalLibrary.org/conference-proceedings-of-spie

Comparison between thermoelastic and ablative induced elastic waves in soft media using ultra-fast line-field low coherent holography

Susobhan Das, Chih-Hao Liu, Alexander Schill, Kirill V. Larin

Susobhan Das, Chih-Hao Liu, Alexander Schill, Kirill V. Larin, "Comparison between thermoelastic and ablative induced elastic waves in soft media using ultra-fast line-field low coherent holography," Proc. SPIE 10496, Optical Elastography and Tissue Biomechanics V, 104960G (19 February 2018); doi: 10.1117/12.2290384

SPIE.

Event: SPIE BiOS, 2018, San Francisco, California, United States

Comparison between thermoelastic and ablative induced elastic waves in soft media using ultra-fast line-field low coherent holography

Susobhan Das[a], Chih-Hao Liu[a], Alexander Schill[a], and Kirill V. Larin[a,b,c,*]
[a]Department of Biomedical Engineering, University of Houston, 3605 Cullen Boulevard, Houston, Texas 77204, USA; [b]Interdisciplinary Laboratory of Biophotonics, Tomsk State University, 36 Lenin Ave., Tomsk 634050, Russia; [c]Molecular Physiology and Biophysics, Baylor College of Medicine, One Baylor Plaza, Houston, Texas 77030, USA

ABSTRACT

Laser induced elastic waves in soft media have great potential to characterize tissue biomechanical properties. The instantaneous increase in local temperature caused by absorption of laser energy leads to a mechanical perturbation in the sample, which can then propagate as a pressure (or an elastic) wave. The generation of the elastic wave can be via thermoelastic or ablative processes depending on the absorption coefficient of the sample and incident laser fluence. It is critical to differentiate between these regimes because only the thermoelastic regime is useful for nondestructive analysis of tissues. To investigate the transition point between these two different regimes, we induced elastic waves in tissue mimicking agar phantoms mixed with different concentrations of graphite powder. The elastic waves were excited by a 532nm pulsed laser with a pulse duration of 6 ns. The fluence of the pulsed laser was tuned from 0.08 J/cm^2 to 3.19 J/cm^2, and the elastic wave was captured by ultra-fast line-field low coherent holography system capable of single-shot elastic wave imaging with nanometer-scale displacement sensitivity. Different concentrations of graphite powder enabled excitation in sample with controlled and variable attenuation coefficient, enabling measurement of the transition between the thermoelastic and ablative regimes. The results show that the transition from thermoelastic to ablative generated waves was 0.75 J/cm^2 and 1.84 J/cm^2 for phantoms with optical attenuation coefficients of 6.64±0.32 mm^{-1} and 26.19±1.70 mm^{-1}, respectively. Our results show promise for all optical biomechanical characterization of tissues.

Keywords: optical elastography, thermoelastic, ablative, holography

1. INTRODUCTION

Optical coherence elastography (OCE) [1, 2] has benefited from advancements in its parent imaging modality, optical coherence tomography (OCT) [3] such as speed [4-6]. However, the most common excitation methods, such as contact [7], acoustic [8-10], or pneumatic [11, 12] stimulation have limitations. For example, contact based methods require careful consideration of tissue type and may not be appropriate for certain applications where direct contact is undesirable. Similarly, acoustic techniques require the use of a coupling medium and may exceed allowable excitation energies. Air based excitation techniques can only excite low frequency responses in tissues, which is susceptible to boundary conditions and limits spatial resolution [13, 14]. Optical excitation may overcome these limitations. Several groups have demonstrated generation of elastic waves in tissue using pulsed lasers [15-21]. The absorption of light induces a rapid increase in the localized temperature and generates a mechanical displacement in the tissue, which can then propagate as an elastic wave through the target tissue. Therefore, this technique shows promise for completely noninvasive all-optical characterization of tissue biomechanical properties. However, generation of elastic waves with sufficiently detectable amplitude can induce damage to tissues and cells [22-27]. To this end, external agents have been proposed to enhance the laser energy absorption, such as gold nanoparticles [28], perfluorocarbon [29], ink [15], and graphite powder [21].

Based on the pulsed laser fluence and the absorption coefficient of the sample at excitation laser wavelength, the generated elastic wave can generally be characterized into two regimes, thermoelastic or ablative [21]. In this work, we experimentally measured the transition point between the two regimes by exciting waves with a 532 nm pulsed laser at various pulse energies in tissue-mimicking agar phantoms with different concentrations of graphite powder. This work is a critical step for developing truly safe noncontact all-optical elastographic techniques.

Optical Elastography and Tissue Biomechanics V, edited by Kirill V. Larin, David D. Sampson, Proc. of SPIE Vol. 10496, 104960G · © 2018 SPIE · CCC code: 1605-7422/18/$18 · doi: 10.1117/12.2290384

2. MATERIALS AND METHODS

A Q-switched, frequency doubled Nd:YAG laser at 532 nm (Polaris II, New Wave Research, Inc.) induced the elastic waves in the samples at various pulse energies, from 0.29 mJ to 12.27 mJ per pulse. The excitation beam was focused on the sample surface with an incidence angle of ~15°. The focused beam diameter on the sample surface was ~0.7 mm, resulting in an incident fluence of 0.08 J/cm^2 to 3.19 J/cm^2. The laser-induced elastic waves were detected using a line field low coherence holography (LF-LCH) imaging system, which has been described previously [30, 31]. The LF-LCH system had a temporal resolution of 5 μs and displacement sensitivity of 1 nm. The focus of the excitation beam was offset from the line focus of the LF-LCH system by ~5 mm. The pulsed laser was externally triggered and synchronized with the LF-LCH system.

To prepare the graphite phantoms (n=3 of each type), we mixed various amounts of graphite power into a 1% (w/w) agar preparation. The absorption coefficient at the pulsed laser wavelength (532 nm) of each sample was determined by measuring the transmittance of 10 slices of phantom of different thicknesses. The mean value and the standard deviation of the measured absorption coefficients for the different phantoms is shown in Table 1.

Table 1. Absorption coefficient of 1% (w/w) agar phantoms mixed with various amounts of graphite powder (n=3 of each type).

Graphite Powder (%)	Absorption Coefficient (mm^{-1})
0.5	6.64±0.32
2.0	26.19±1.70

3. RESULTS & DISCUSSION

The temporal profiles of the elastic waves induced by either the thermoelastic or ablative processes have distinguishing features as shown in Figure 1. In the thermoelastic regime, the wave has two distinct peaks with equal but opposite amplitudes as indicated in Figure 1(a). On the other hand, the ablative regime has asymmetric displacement in positive and negative direction, but is nearly symmetric about the center of the maximal negative displacement as shown in Figure 1(b).

Moreover, the elastic wave amplitude and group velocity were analyzed as per our previous publications [30-33]. The Young's modulus of all the samples were also measured by the "gold standard" uniaxial mechanical testing (Model 5943, Instron Corp., MA, USA) as 20±5 kPa. The measured elastic wave group velocity for all concentration of graphite phantom was 2.18±0.2 m/s, which translates to 17.8±3 kPa as estimated by the surface wave equation, which is in agreement with our previous work [34] and mechanical testing.

The dependence of the elastic wave amplitude as a function of laser energy was investigated by gradually increasing the excitation laser energy from 0.29 mJ to 12.27 mJ. Shear wave amplitudes were averaged for each energy on three samples of each graphite concentration. The excitation location was changed after each measurement to avoid any potential local degradation of the medium.

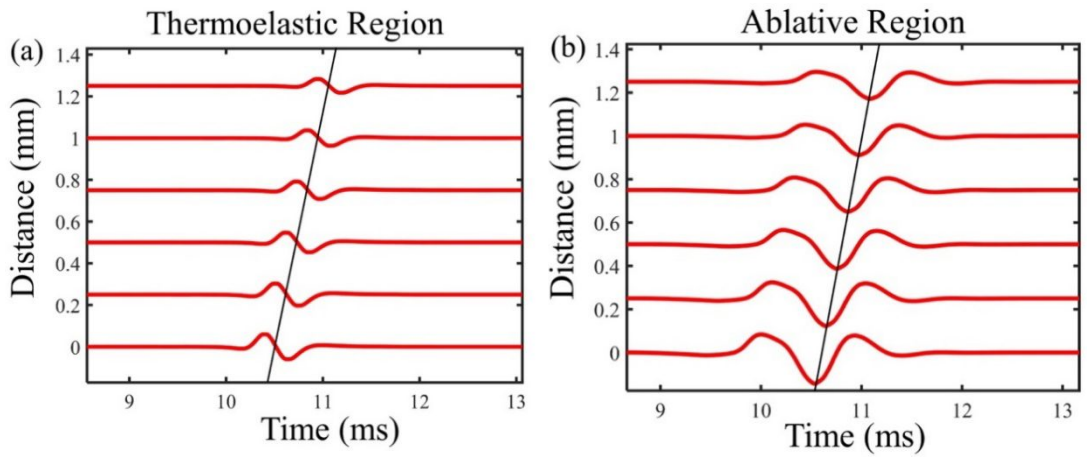

Figure 1. Temporal profile of laser induced elastic wave in (a) thermoelastic regime and (b) ablative regime at different distance of propagation.

The elastic wave amplitude was measured as the mean squared amplitude of the displacement up to 0.1 mm from the start of the imaging region as measured from the phantom surface by the LF-LCH system. Sample measurements are illustrated in Figure 2. The results show that as we increased the excitation pulse energy, the transition from the thermoelastic to ablative regime occurred after a certain pulsed laser energy that was determined by the absorption coefficient of the sample. The transition point from thermoelastic regime to ablative regime is marked by correspondingly colored arrows for the two typical samples with different absorption coefficients in Figure 2. The elastic waves generated by the pulsed laser energy to the left of the arrows were excited in the corresponding thermoelastic regime and the waves to the right were induced in the ablative regime. Clearly, the transition point increased in energy as the absorption coefficient increased, which was as expected. Moreover, the slope of shear wave amplitude versus laser pulse energy beyond the transition point (i.e. ablative regime) is much steeper than the slope in thermoelastic regime. Previous work has suggested that this is due to the nonlinear nature of the ablation process [35].

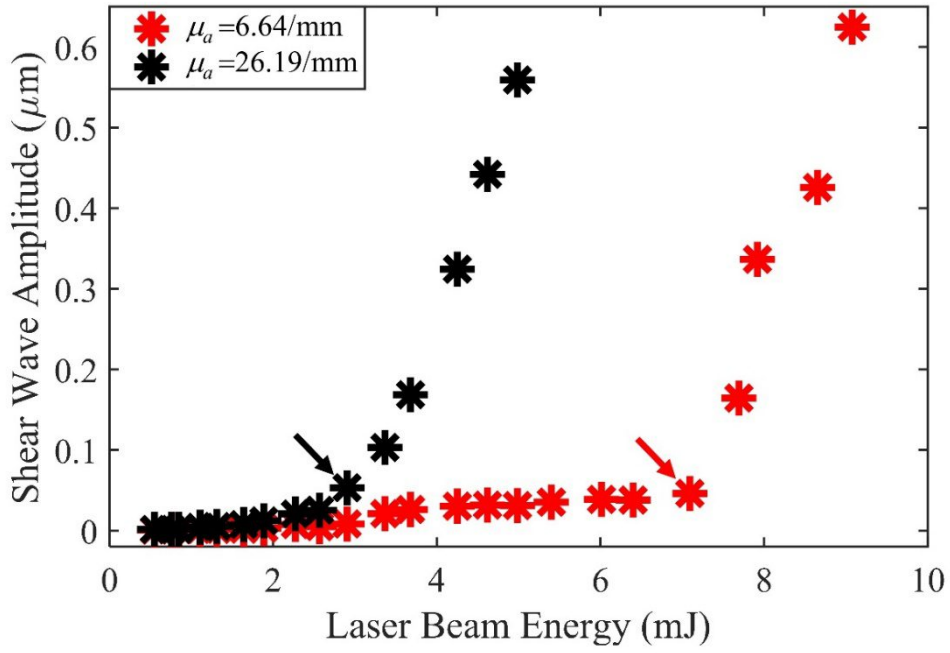

Figure 2. Shear wave amplitude for different phantom samples with various attenuation coefficients as a function of excitation energy. The transition point from thermoelastic to ablative regime is marked by the correspondingly colored arrows.

4. CONCLUSIONS

We investigated the excitation of elastic waves in tissue-mimicking agar phantoms mixed with various amounts of graphite powder. The excitation energy of the 532nm pulsed laser was incrementally adjusted, and the resulting waves were detected by a line-field low coherence holography system. The elastic wave amplitudes increased as a function of excitation pulse energy, and a clear transition point between thermoelastic and ablative induced elastic waves was observed. Moreover, the required incident energy to transition from the thermoelastic to ablative excitation regimes decreased as a function of the optical absorption coefficient. Our future work will investigate a larger range of optical absorption coefficients and stiffnesses. Our work is a critical step for developing safe and completely noncontact all-optical elastography.

ACKNOWLEDGEMENTS

This work was supported, in part, by the U.S. National Institutes of Health (NIH) Grant Nos. 2R01EY022362, 1R01HL120140, and U54HG006348 and U.S. Department of Defense (DOD) Congressionally Directed Medical Research Programs (CDMRP) Grant No. PR150338. The authors would like to thank Manmohan Singh with the Department of Biomedical Engineering at the University of Houston for his technical advice and aid in drafting this manuscript.

REFERENCES

[1] J. Schmitt, "OCT elastography: imaging microscopic deformation and strain of tissue," Opt Express, 3(6), 199-211 (1998).

[2] K. V. Larin, and D. D. Sampson, "Optical coherence elastography - OCT at work in tissue biomechanics [Invited]," Biomed Opt Express, 8(2), 1172-1202 (2017).

[3] D. Huang, E. A. Swanson, C. P. Lin *et al.*, "Optical coherence tomography," Science, 254(5035), 1178-81 (1991).

[4] R. Huber, D. C. Adler, and J. G. Fujimoto, "Buffered Fourier domain mode locking: unidirectional swept laser sources for optical coherence tomography imaging at 370,000 lines/s," Opt Lett, 31(20), 2975-2977 (2006).

[5] R. Huber, M. Wojtkowski, and J. G. Fujimoto, "Fourier Domain Mode Locking (FDML): A new laser operating regime and applications for optical coherence tomography," Opt Express, 14(8), 3225-37 (2006).

[6] T. Klein, and R. Huber, "High-speed OCT light sources and systems [Invited]," Biomedical Optics Express, 8(2), 828-859 (2017).

[7] K. M. Kennedy, L. Chin, R. A. McLaughlin *et al.*, "Quantitative micro-elastography: imaging of tissue elasticity using compression optical coherence elastography," Sci Rep, 5, 15538 (2015).

[8] J. Zhu, L. Qi, Y. Miao *et al.*, "3D mapping of elastic modulus using shear wave optical micro-elastography," Sci Rep, 6, 35499 (2016).

[9] T. M. Nguyen, B. Arnal, S. Song *et al.*, "Shear wave elastography using amplitude-modulated acoustic radiation force and phase-sensitive optical coherence tomography," J Biomed Opt, 20(1), 016001 (2015).

[10] C. Wu, Z. Han, S. Wang *et al.*, "Assessing age-related changes in the biomechanical properties of rabbit lens using a coaligned ultrasound and optical coherence elastography system," Invest Ophthalmol Vis Sci, 56(2), 1292-300 (2015).

[11] S. Wang, K. V. Larin, J. S. Li *et al.*, "A focused air-pulse system for optical-coherence-tomography-based measurements of tissue elasticity," Laser Phys Lett, 10(7), 075605 (2013).

[12] C. Dorronsoro, D. Pascual, P. Perez-Merino *et al.*, "Dynamic OCT measurement of corneal deformation by an air puff in normal and cross-linked corneas," Biomed Opt Express, 3(3), 473-87 (2012).

[13] S. Wang, and K. V. Larin, "Noncontact depth-resolved micro-scale optical coherence elastography of the cornea," Biomed Opt Express, 5(11), 3807-21 (2014).

[14] Z. Han, J. Li, M. Singh *et al.*, "Optical coherence elastography assessment of corneal viscoelasticity with a modified Rayleigh-Lamb wave model," J Mech Behav Biomed Mater, 66, 87-94 (2017).

[15] C. Li, G. Guan, Z. Huang *et al.*, "Noncontact all-optical measurement of corneal elasticity," Opt Lett, 37(10), 1625-7 (2012).
[16] S. Song, W. Wei, B. Y. Hsieh *et al.*, "Strategies to improve phase-stability of ultrafast swept source optical coherence tomography for single shot imaging of transient mechanical waves at 16 kHz frame rate," Appl Phys Lett, 108(19), 191104 (2016).
[17] A. G. Doukas, and T. J. Flotte, "Physical characteristics and biological effects of laser-induced stress waves," Ultrasound Med Biol, 22(2), 151-64 (1996).
[18] M. L. Dark, L. T. Perelman, I. Itzkan *et al.*, "Physical properties of hydrated tissue determined by surface interferometry of laser-induced thermoelastic deformation," Phys Med Biol, 45(2), 529-39 (2000).
[19] J. Noack, and A. Vogel, "Single-shot spatially resolved characterization of laser-induced shock waves in water," Appl Opt, 37(19), 4092-9 (1998).
[20] G. Paltauf, and H. Schmidt-Kloiber, "Measurement of laser-induced acoustic waves with a calibrated optical transducer," Journal of Applied Physics, 82(4), 1525-1531 (1997).
[21] P. Grasland-Mongrain, Y. Lu, F. Lesage *et al.*, "Generation of shear waves by laser in soft media in the ablative and thermoelastic regimes," Applied Physics Letters, 109(22), 221901 (2016).
[22] S. Thomsen, "Pathologic analysis of photothermal and photomechanical effects of laser-tissue interactions," Photochem Photobiol, 53(6), 825-35 (1991).
[23] Y. Yashima, D. J. McAuliffe, S. L. Jacques *et al.*, "Laser-induced photoacoustic injury of skin: effect of inertial confinement," Lasers Surg Med, 11(1), 62-8 (1991).
[24] A. Sonden, B. Svensson, N. Roman *et al.*, "Laser-induced shock wave endothelial cell injury," Lasers Surg Med, 26(4), 364-75 (2000).
[25] A. G. Doukas, D. J. McAuliffe, and T. J. Flotte, "Biological effects of laser-induced shock waves: structural and functional cell damage in vitro," Ultrasound Med Biol, 19(2), 137-46 (1993).
[26] A. L. McKenzie, "Physics of thermal processes in laser-tissue interaction," Phys Med Biol, 35(9), 1175-209 (1990).
[27] A. G. Doukas, D. J. McAuliffe, S. Lee *et al.*, "Physical factors involved in stress-wave-induced cell injury: the effect of stress gradient," Ultrasound Med Biol, 21(7), 961-7 (1995).
[28] M. A. van Dijk, M. Lippitz, and M. Orrit, "Detection of acoustic oscillations of single gold nanospheres by time-resolved interferometry," Phys Rev Lett, 95(26), 267406 (2005).
[29] E. Strohm, M. Rui, I. Gorelikov *et al.*, "Vaporization of perfluorocarbon droplets using optical irradiation," Biomed Opt Express, 2(6), 1432-1442 (2011).
[30] C. H. Liu, A. Schill, R. Raghunathan *et al.*, "Ultra-fast line-field low coherence holographic elastography using spatial phase shifting," Biomed Opt Express, 8(2), 993-1004 (2017).
[31] C. H. Liu, A. Schill, C. Wu *et al.*, "Non-contact single shot elastography using line field low coherence holography," Biomed Opt Express, 7(8), 3021-31 (2016).
[32] J. Li, Z. Han, M. Singh *et al.*, "Differentiating untreated and cross-linked porcine corneas of the same measured stiffness with optical coherence elastography," J Biomed Opt, 19(11), 110502 (2014).
[33] S. Wang, A. L. Lopez, 3rd, Y. Morikawa *et al.*, "Noncontact quantitative biomechanical characterization of cardiac muscle using shear wave imaging optical coherence tomography," Biomed Opt Express, 5(7), 1980-92 (2014).
[34] Z. Han, J. Li, M. Singh *et al.*, "Quantitative methods for reconstructing tissue biomechanical properties in optical coherence elastography: a comparison study," Phys Med Biol, 60(9), 3531-47 (2015).
[35] C. Li, Z. Huang, and R. K. Wang, "Elastic properties of soft tissue-mimicking phantoms assessed by combined use of laser ultrasonics and low coherence interferometry," Opt Express, 19(11), 10153-63 (2011).